Int. J. Heat Mass Transfer. Vol. 9, pp. 53–61. Pergamon Press 1966. Printed in Great Britain

FREE CONVECTION IN AN AIR–WATER VAPOR BOUNDARY LAYER

E. M. SPARROW, J. W. YANG and C. J. SCOTT

Heat Transfer Laboratory, Department of Mechanical Engineering, University of Minnesota, Minneapolis, Minnesota

(*Received* 19 *March* 1965 *and in revised form* 19 *July* 1965)

Abstract—This paper describes an experimental investigation, supported by analysis, of free convection in an air–water vapor boundary layer at the stagnation point of a horizontal cylinder. A two-component boundary layer is created by the effusion of water vapor from the porous surface of the cylinder; the ambient gas is pure air. The results of both experiment and analysis indicate that the heat transfer decreases as the surface mass-transfer rate increases. At moderate blowing rates, there is good agreement between the experimentally- and analytically-determined Nusselt numbers. At higher mass-transfer rates, the data lie above the analytical predictions by about 25 per cent. This departure is attributed to a fluctuating motion in the boundary layer.

NOMENCLATURE

g, acceleration of gravity;
h, heat-transfer coefficient;
i, specific enthalpy of steam;
k, thermal conductivity;
$\dot{m}$, mass-transfer rate/time-area;
Nu, Nusselt number;
q_{cond}, conductive heat flux;
q_{rad}, radiative heat flux;
q_w, convective heat flux;
r, cylinder radius;
T, absolute temperature;
W_{H_2O}, mass fraction of steam at surface.

Greek symbols
β, coefficient of thermal expansion;
ϵ, emittance;
ν, kinematic viscosity;
ρ, density;
σ, Stefan–Boltzmann constant.

Subscripts
aw, adiabatic wall;
e, radiation environment;
o, interior of test section;
w, cylinder surface;
∞, ambient air.

INTRODUCTION

BOUNDARY LAYER flows involving mixtures of air and water vapor may be found in many branches of technology. For instance, such flows may occur in the condensation of steam when air (a noncondensable) is present, in the humidification and dehumidification of air, and in a variety of chemical process operations. Recently, it has been suggested that the injection of steam through a porous surface into a hot air stream may be an effective means of surface thermal protection (i.e. mass-transfer cooling).

Upon consideration of the literature, it appears that such boundary layers have not yet been subjected to controlled experimental study. The present paper describes an experimental investigation, supported by analysis, of the air–water vapor boundary layer in a free-convection flow about a horizontal cylinder. The two-component boundary layer is created by passing steam from the interior of the cylinder out through pores in the cylinder surface; the cylinder is situated in an otherwise quiescent air environment. The measurements are concerned specifically with the heat-transfer characteristics at the stagnation point of the cylinder. These results are directly comparable to stagnation-point solutions of the complete momentum, energy, and diffusion equations.

In the presentation that follows, a description will first be given of the experimental apparatus, with particular emphasis on the steam system.

Then, the data reduction procedure will be outlined. Next, the experimental results are presented, discussed and compared with those of analysis. Finally, additional analytical results will be given.

THE EXPERIMENTAL APPARATUS AND ITS OPERATION

The description of the experimental apparatus is facilitated by reference to Fig. 1, which shows a schematic diagram of the main elements of the system. Saturated steam at approximately 300°F is generated in a boiler* and passes through a pressure regulator and reducing valves to a superheater. The flow rate of the thus superheated steam is then measured by a calibrated orifice. Next, the steam passes through a second superheater which facilitates the adjustment of the test-section temperature. From the superheater, the flow enters the interior of the test section and then diffuses out through the porous wall into the boundary layer. All piping in the system was wrapped with fiberglass insulation.

The test section itself is a porous cylindrical shell, 3 inches in diameter and 12 inches in length. The shell is made of woven stainless-steel cloth that consists of two layers of woven-wire mesh, bonded together by a sintering and rolling process. The thickness of the porous wall is about 0·035 in. For purposes of support and isolation, the ends of the test cylinder are fitted with a pair of hollow Lucite cylinders, each 3 inches in diameter and 8 inches in length.

With a view toward achieving a uniform effusion of the steam through the surface, the stainless-steel shell is internally lined with an annulus of fiberglass filter paper of $\frac{1}{8}$ in thickness. The steam is introduced into the interior of the test section through a $\frac{1}{2}$ in diameter perforated tube that runs coaxially through the entire length of the porous cylinder.

Wall temperature measurements were accomplished with thermocouples welded to the inside surface of the porous shell. The thermocouple wire is iron–constantan, 36-gage. At the outset of the tests, there were a total of 40 such thermocouples, circumferentially distributed in a plane midway between the ends of the cylinder and in a pair of planes 2 in distant from the mid-plane. During the course of the experiment, many of the thermocouple junctions became inoperative due to the corrosive action of the steam.† Fortunately, a sufficient number of thermocouples in the stagnation region of the mid-plane continued operative throughout the entire duration of the tests. The temperature of the steam in the interior of the test section was sensed by thermocouples suspended in the

* Model ES 12, Automatic Steam Products Corporation.

† The model had initially been designed to accommodate non-corrosive gases, and the thermocouple material was chosen accordingly.

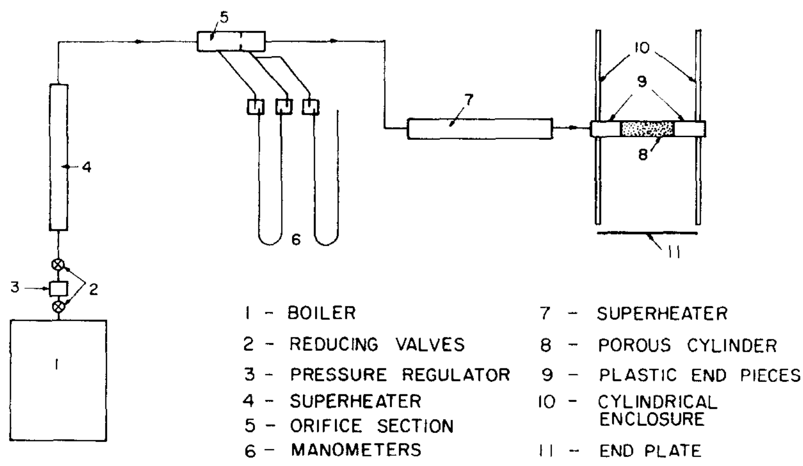

FIG. 1. The experimental apparatus.

openings of the delivery tube at several locations along its length. All thermocouple voltages were detected by a Brown Electronik self-balancing potentiometer.

As indicated in Fig. 1, the test section is mounted horizontally in a hollow-walled cylindrical enclosure, 4 ft high and 2 ft in diameter. The bottom of the enclosure is partially closed with a circular plate, the primary function of which is to provide a known environment for radiant interchange with the lower stagnation region of the test section. The surface of the cylindrical enclosure and the end plate are both black. Thermocouples were affixed at various locations on the aforementioned surfaces. The air temperature at several positions within the cylindrical enclosure was sensed by shielded thermocouples.

In a further effort to achieve quiescent environmental conditions, the aforementioned cylindrical enclosure was housed in an enclosed space that is segregated by partitions from the remainder of the laboratory room. However, the partitions do not fully extend to the floor or to the ceiling; thus, air can be exchanged between the enclosed space and the room.

As was previously noted, the measurement of the steam flow rate is accomplished by employing a calibrated orifice. The orifice plate, fabricated according to ASME standards, has a hole diameter of $\frac{1}{8}$ in and is situated in a tube of $\frac{7}{16}$ in diameter. Pressure taps are located one diameter upstream and one-half diameter downstream of the orifice plate. Temperatures were also measured upstream and downstream of the orifice. The calibration was accomplished by ducting steam from the downstream end of the orifice section through a condenser. The condensate collected in a given period of time was weighed on a precision balance. It is believed that the orifice calibration is accurate to ± 1 per cent.

The measurement of the steam pressures upstream and downstream of the orifice was accomplished by employing a specially designed manometer system. The manometer arrangement will now be discussed with the aid of Fig. 2. The pressures p_1 and p_2 respectively represent the upstream and downstream pressures.

For the measurement of the differential pressure $p_1 - p_2$, one employs a U-tube as shown in the left-hand portion of the diagram. The top of each leg of the U-tube is connected to a separate glass chamber. Each chamber is

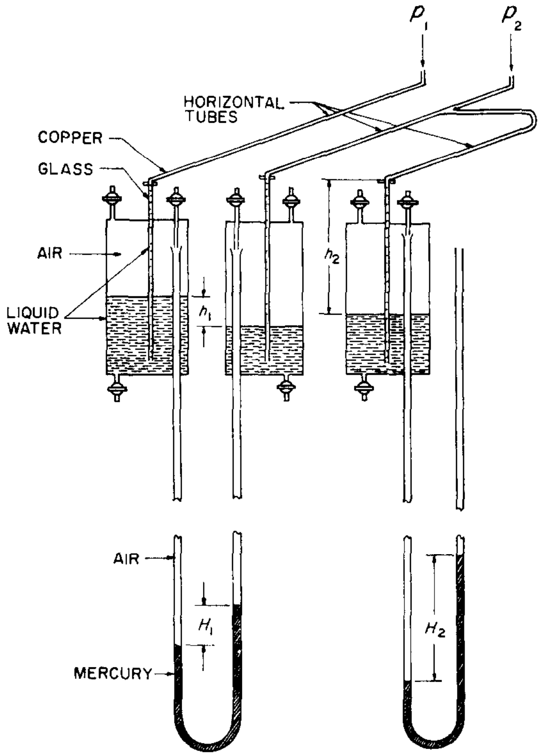

FIG. 2. Manometer system for measuring steam pressure.

partly filled with liquid water. The space above the water is filled with air, and the U-tube protrudes into the air space. The pressures p_1 and p_2 are conveyed to the respective chambers through horizontal copper tubes which are joined to glass tubes at the tops of the chambers. Under test conditions, the interface between the steam and the liquid water is located somewhere within the copper tube, both for the p_1 and the p_2 sides of the manometer. This is the essential feature in the operation of the manometer. Under this condition, it can readily be derived that

$$p_1 - p_2 = \rho_{\mathrm{Hg}}\, g\, H_1 + \rho_{\mathrm{H_2O}}\, g\, h_1 \qquad (1)$$

The measurement of the absolute pressure p_2 is illustrated in the right-hand portion of Fig. 2.

In this instance, one leg of the manometer is open to the atmosphere. Once again, the essential feature of the operation is that the interface between the steam and the liquid water be located in the horizontal copper tube. Correspondingly, one finds

$$p_2 - p_\infty = \rho_{\mathrm{Hg}}\, g\, H_2 - \rho_{\mathrm{H_2O}}\, g\, h_2. \qquad (2)$$

The U-tubes are approximately 60 inches in length. The glass chambers are $1\frac{1}{2}$ inches in diameter and 3 inches long.

In carrying out the experiments, care had to be exercised to prevent condensation of steam in the test section. To this end, as a prelude to initiating the steam flow, hot air was passed through the system for about 1 h. At the end of this period, a temperature of 250–300°F was achieved in the test section. Then, the steam flow was actuated, and, after an additional period of 2 h, steady-state operation was achieved and data were collected.

Structural limitations of the apparatus precluded a wide range in the values of the wall temperature. For this reason and also to facilitate comparison with the analytical solutions (which contain as a parameter the ratio of wall temperature to environment temperature), it was deemed desirable to run all the tests at approximately a fixed wall temperature. Thus, the blowing rate of the steam is the principle independent variable of the experimental investigation. Analytical results are given for a range of thermal boundary conditions.

REDUCTION OF DATA

The determination of the local heat-transfer rate at the stagnation point is accomplished by setting up an energy balance. In this connection, it is convenient to envision a control volume at the stagnation point that spans the porous steel shell and the fiberglass liner. Under steady-state conditions, the application of the energy conservation principle to such a control volume yields

$$\dot{m}\,(i_o - i_w) = q_w + q_{\mathrm{rad}} + q_{\mathrm{cond}}. \qquad (3)$$

The left-hand side of this expression is the enthalpy change sustained by the steam as it passes from the interior of the test section to the surface. The symbols i_o and i_w represent the enthalpy of steam in the interior and at the surface, while $\dot{m}$ is the steam flow rate per unit surface area.

There are three heat-flux terms appearing on the right-hand side. The first of these, q_w, is the convective heat transfer from the wall to the boundary layer. The second is the net radiative transport between the porous shell and the surroundings, while the last represents losses by heat conduction from the control volume. All heat fluxes are per unit surface area.

The enthalpy rise term is evaluated by employing the steam flow rate from the orifice and the temperatures T_o and T_w respectively measured in the interior of the model and on the porous stainless-steel shell. Typically, T_w was approximately 695°R (235°F), while T_o ranged from 760°R (300°F) to 800°R (340°F). The corresponding enthalpies* i_o and i_w were read from the *Steam Tables* [1]. It is assumed that the steam emerging from the surface of the cylinder is at the same temperature as the stainless-steel shell.

The net transport of radiation from the porous surface to the black-walled surroundings (temperature T_e) is calculable from the relationship

$$q_{\mathrm{rad}} = \epsilon\sigma\,(T_w^4 - T_e^4) \qquad (4)$$

in which T_w is the measured temperature at the stagnation point and ϵ is the surface emittance. From an independent experiment described in reference 2, it was determined that $\epsilon = 0{\cdot}407$. Over the range of blowing rates of this investigation, q_{rad} ranged from 45 to 55 per cent of the enthalpy rise, with the higher values corresponding to higher blowing rates. Radiation contributions of this magnitude are altogether reasonable when free convection is the only alternate mode of heat transport.

The conduction losses were fully negligible in the present experiment, especially since consideration is being given to a thermally symmetric location such as the stagnation point.

In the light of the foregoing discussion, all terms of equation (3) except q_w are directly

* In evaluating i_w, the partial pressure of the steam was taken from the analytical solutions that are discussed later.

evaluable from the measured data. Thus, q_w can be determined from the difference between the enthalpy rise and the radiation flux. With the q_w values thus obtained, a local heat-transfer coefficient h is computed from the definition

$$h = \frac{q_w}{T_w - T_\infty} \tag{5}$$

The thermal driving force employed in the foregoing definition is $(T_w - T_\infty)$. In this connection, it may be noted that in two-component boundary layers, thermal diffusion effects may operate to create a condition whereby $T_w \neq T_\infty$ when $q_w = 0$ (see, for instance, reference 2). In such cases, an appropriate driving force is $(T_w - T_{aw})$, where T_{aw} is the adiabatic wall temperature (that is, the wall temperature corresponding to $q_w = 0$).

For the air–water vapor boundary layer, analysis shows that the thermal diffusional effects are of secondary importance for the temperature differences and flow rates of this experiment. Moreover, owing to the onset of condensation, the adiabatic wall temperatures are not measureable. Additionally, the adiabatic wall temperatures predicted by analysis are prone to some uncertainty because the thermal diffusion factor is not known to within a factor of two [3]. In this light, it was deemed altogether reasonable to omit further consideration of the adiabatic wall temperature in the data reduction and to employ $(T_w - T_\infty)$ as the thermal driving force.

The heat-transfer results are reported in terms of the dimensionless representation

$$Nu \Big/ \sqrt{\left[\frac{r\,(gr)^{\frac{1}{2}}}{\nu_\infty}\right]}, \qquad Nu = \frac{hr}{k_\infty} \tag{6}$$

where r is the cylinder radius and g is the acceleration of gravity. The particular form of the foregoing dimensionless grouping is suggested by analysis [4]. It may be observed that $(gr)^{\frac{1}{2}}$ has the dimensions of a velocity*, and correspondingly, $r(gr)^{\frac{1}{2}}/\nu_\infty$ is similar to a Reynolds number. A dimensionless mass injection parameter is also suggested by analysis

$$\frac{\dot{m}}{\rho_\infty\,(gr)^{\frac{1}{2}}} \sqrt{\left[\frac{r\,(gr)^{\frac{1}{2}}}{\nu_\infty}\right]} \tag{7}$$

It is readily verified that the foregoing has the same form as the blowing parameter for forced-convection mass-transfer cooling. In this investigation, $\dot{m}$ ranged from 4·1 to 7·8 lb/h ft^2, and this resulted in a range of the mass injection parameter from 0·3 to 0·58.

RESULTS AND DISCUSSION

The experimentally determined Nusselt numbers are plotted as open circles in Fig. 3 with

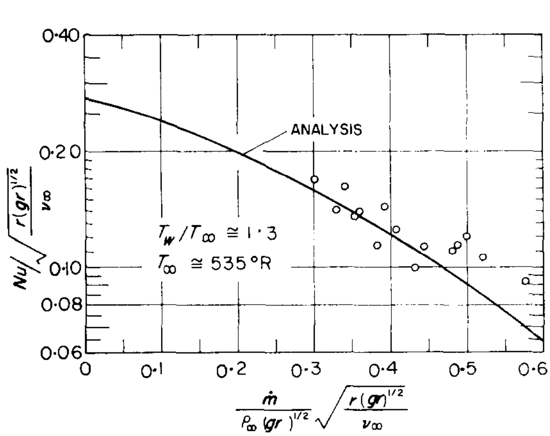

FIG. 3. Experimental and analytical heat-transfer results.

the dimensionless mass-transfer rate as independent variable. Also appearing in the figure is a solid line representing the prediction of analysis (the details of the analysis will be discussed later).

The experimental conditions were such that the ambient temperature T_∞ was approximately 535°R (75°F). In the majority of the runs, the temperature ratio T_w/T_∞ had a value of 1·3. For three of the tests, T_w/T_∞ took on values between 1·31 and 1·325. The Nusselt numbers for these points were corrected by 1–2 per cent in accordance with theory. The experiments were performed under low-humidity environmental conditions, the mass fraction of water vapor in the environment being 0·008 or less.

The analytical curve shown in the figure

* The analysis takes account of variable fluid properties. Consequently, the factor $\beta(T_w - T_\infty)$ does not naturally arise in the velocity grouping as for a constant property fluid.

corresponds to the thermal conditions

$$T_\infty = 535^\circ\mathrm{R} \text{ and } T_w/T_\infty = 1{\cdot}3$$

and to an ambient gas that is pure air. However, it was verified that this curve continues to apply without perceptible change for cases in which the water vapor content of the environment is as much as 2 per cent (mass fraction). Furthermore, within the scale of the figure this same curve represents the heat-transfer results calculated both with and without the thermal diffusional effects. In the former case, the heat-transfer coefficient is defined with $(T_w - T_{aw})$ as the thermal driving force; in the latter case, $(T_w - T_\infty)$ is used as the thermal driving force.

Inspection of the figure indicates that the effect of increased surface mass transfer is to decrease the convective Nusselt number. This trend is consistent with prior experience with mass transfer cooling in forced-convection flows. However, as will be demonstrated later, the opposite trend can sometimes occur in free-convection flows.

At the lower mass-transfer rates, the experimental data scatter both above and below the analytical prediction. The extent of the scatter, which is about ± 10 per cent about a mean line, is in no way excessive when it is recalled that the radiation correction amounts to approximately 50 per cent of the overall heat-transfer rate. It appears altogether reasonable to conclude that the analytical results are well confirmed by experiment in the range of moderate blowing rates.

At the higher mass-transfer rates, the data points show greater deviations from the analytical curve. As will be developed in the forthcoming discussion, these deviations are attributable to departures of the operating conditions from the steady, laminar flow postulated in the analysis.

During the course of the experiments, visual observations of the up-facing portion of the test section were made from a suitably arranged platform. For all operating conditions, one could see the following: adjacent to the porous surface, there was a clear layer of gas; farther from the surface, a layer containing fog particles was in evidence. Such a fog layer was observed for all the blowing rates investigated. Moreover, it was present during the final runs (performed under low-humidity conditions) as well as during preliminary runs performed under high-humidity conditions. At the present time, the authors are unable to provide further information on the mechanism of the fog formation. The analytical model does not take cognizance of fog formation.

In view of Fig. 3, one may conclude that the fog layer did not have a first-order effect on the heat-transfer results. However, it did serve quite effectively as an agent for flow visualization. Thus, at low rates of mass transfer, the fog film was seen to be basically stable, but with an occasional lazy wave motion. At high mass-transfer rates, the oscillations of the fog layer were stronger and more frequent. It appeared quite plausible to the observer that such unsteadiness could well augment the heat-transfer rates relative to those for a steady, laminar flow pattern.

In light of the foregoing discussion, it may be concluded that the analytical prediction can be applied with confidence in the range of small and moderate mass-transfer rates. At higher rates of mass transfer, the analytical predictions appear to be conservative by about 25 per cent. It should also be noted that stagnation-point heat-transfer results apply without essential change in a substantial adjacent region on the cylinder surface. Present measurements, as well as those of prior investigations (e.g. reference 2), suggest that the stagnation point results can be applied over a length of arc subtending 45° to each side of the stagnation point.

It may be of interest to consider the concentrations of water vapor at the cylinder surface that correspond to the mass-transfer rates of the present investigation. This information has been determined from the aforementioned analytical solutions and is presented in the lower portion of Fig. 4 as the curve corresponding to $T_w/T_\infty = 1{\cdot}3$. The ordinate W_{H_2O} is the mass fraction of water vapor at the cylinder wall, while the abscissa is the mass-transfer parameter. Inspection of the figure reveals that the water vapor concentration increases with increasing mass transfer rate. For the range of mass-transfer rates of this investigation, the mass fraction of water vapor ranges from 0·52 to 0·78.

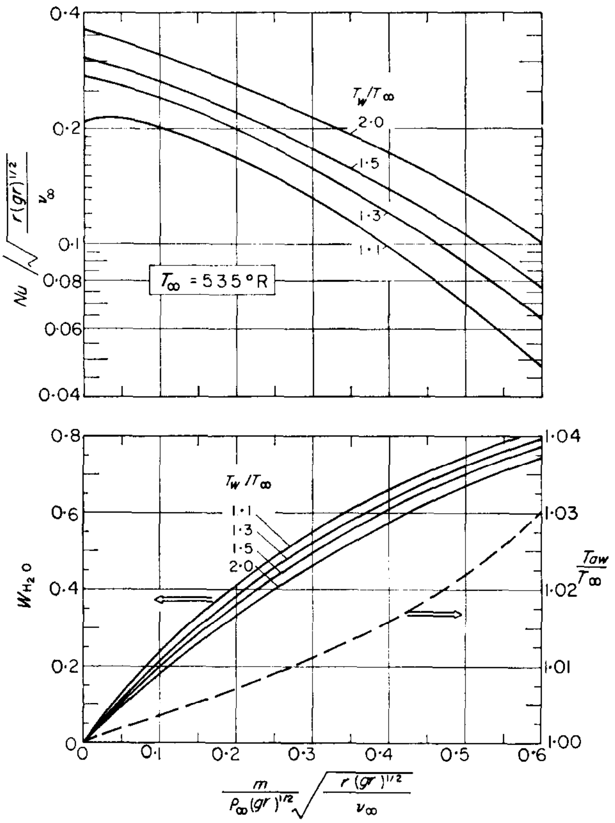

FIG. 4. Analytical results for a range of thermal boundary conditions.

Additional analytical results

The analytical results alluded to in the foregoing section of the paper are based on solutions of the complete momentum, energy, and diffusion equations. The boundary-layer approximations were not utilized. The practicability of dealing with the complete conservation equations is one of the attractive features of working with stagnation-point flows.

The analytical formulation of the problem follows the same lines as was discussed in reference 4 for the helium–air free-convection boundary layer. Consequently, to conserve space, the governing equations will not be repeated here. A necessary ingredient for the solution of these equations is a knowledge of the thermodynamic and transport properties of air, water vapor, and mixtures thereof. The properties of pure air are well documented for the temperature range of this investigation. However, the transport properties of steam and in particular, of air–steam mixtures, are somewhat uncertain. The latter properties were taken from a very recent paper by Mason and Monchick [3].

The numerical solution of the governing conservation equations is a formidable undertaking, even for a high-speed digital computer. This is because of the lengthy and complex representations of the fluid properties and of the intercoupling between the governing equations. The numerical work was performed on a Control Data 1604 computer at the Numerical Analysis Center of the University of Minnesota.

The analytical results thus obtained are presented in Fig. 4. The upper part of the figure pertains to the Nusselt number. The solid lines in the lower portion of the figure provide information on the mass fraction of water vapor at the cylinder surface; the dashed curve gives results for the adiabatic wall temperature which is created by thermal diffusional effects. These results are plotted as a function of the mass-transfer parameter for parametric values of T_w/T_∞. The environment temperature is 535°R; however, the results are quite insensitive to the value of T_∞ over a moderate range.

Upon considering the heat-transfer results, it is seen that the Nusselt numbers generally decrease with increasing mass-transfer rate. This is due to the thickening of the boundary layer that results from mass injection. However, the aforementioned trend is reversed at small blowing rates for $T_w/T_\infty = 1{\cdot}1$.

To illuminate this finding, it may be observed that there are two opposing effects of the surface mass transfer. One of these is to thicken the boundary layer. The other is to augment the buoyancy force by adding a light-weight component to the boundary layer. When the temperature differences of the problem are sufficiently large, the temperature-induced buoyancy force overshadows the concentration-induced buoyancy force. However, when the temperature differences are relatively small, the concentration-induced buoyancy may augment the velocities of the problem so as to cause an increase in heat transfer. This increase persists only until the thickening effect of the surface mass transfer takes over.

The molecular weight of water vapor is only moderately different from that of air. Consequently, the effects of the concentration-induced buoyancy are much smaller than those associated with the injection of a very light gas such as helium. The minor role of the concentration-induced buoyancy in the case of steam injection is further exemplified by the appreciable spread among the Nusselt number curves of Fig. 4 as a function of the temperature ratio T_w/T_∞. On the other hand, for the case of helium injection, corresponding Nusselt number results show only a weak dependence on the temperature ratio [4].

For all cases, the mass fraction of water vapor at the surface, W_{H_2O}, increases with increasing mass-transfer rate. At a given value of the mass-transfer parameter, larger values of W_{H_2O} correspond to smaller values of T_w/T_∞.

Within the scale of the figure, the same curves for Nu and W_{H_2O} represent results from two different sets of solutions; in one set, the thermal diffusional effects have been fully included, while in the other set, these diffusional effects were suppressed. In the former case, the heat-transfer coefficient is defined with $(T_w - T_{aw})$ as the thermal driving force; while in the latter, $(T_w - T_\infty)$ is the thermal driving force.

The adiabatic wall temperature ratios presented in the bottom portion of the figure show a much smaller departure from unity than was previously found for injection of light gases such as helium and hydrogen [2, 4]. Moreover, these results are of somewhat uncertain accuracy owing to appreciable uncertainties in the magnitudes of the thermal diffusion factor for air–water vapor mixtures.

CONCLUDING REMARKS

The general good agreement between analysis and experiment in the range of moderate blowing rates has interesting implications in the theory of mass transfer cooling. This is because in this range, analysis for forced-convection flows [5, 6] predicts that water vapor is a better mass transfer coolant than is helium. This is in contradistinction to the simple rule that arranges the effectiveness of a coolant gas according to its molecular weight, the effectiveness being greater at lower molecular weights.

ACKNOWLEDGEMENTS

The research described herein was supported by a grant from the U.S. Air Force Office of Scientific Research, Mechanics Division. The authors are indebted to Professor E. R. G. Eckert for incisive discussion, and to Mr. W. J. Minkowycz for assistance with the computer operations.

REFERENCES

1. J. H. Kennan and F. G. Keyes, *Thermodynamic Properties of Steam*. John Wiley, New York (1946).
2. E. M. Sparrow, C. J. Scott, R. J. Forstrom and W. A. Ebert, Experiments on the diffusion-thermo effect in a binary boundary layer with injection of various gases, *J. Heat Transfer* **87**, 321–328 (1965).
3. E. A. Mason and L. Monchick, Survey of the equation of state and transport properties of moist gases, in *Proceedings of the* 1963 *International Symposium on Humidity and Moisture*. Reinhold, New York (1965).
4. E. M. Sparrow, W. J. Minkowycz and E. R. G. Eckert, Transpiration-induced buoyancy and thermal diffusion–diffusion thermo in a helium–air free-

convection boundary layer, *J. Heat Transfer* **86**, 508–514 (1964).

5. D. G. HURLEY, Mass transfer cooling in a boundary layer, *Aeronaut. Q.* **12**, 165–188 (1961).
6. E. M. SPARROW, Recent studies relating to mass transfer cooling, *Proceedings of the* 1964 *Heat Transfer and Fluid Mechanics Institute*, pp. 1–18. Stanford University Press (1964).

Résumé—Cet article décrit une étude expérimentale, confirmée par la théorie, de la convection naturelle dans une couche limite d'un mélange d'air et de vapeur d'eau au point d'arrêt d'un cylindre circulaire. La couche limite à deux constituants est créée par l'effusion de la vapeur d'eau à partir de la surface poreuse du cylindre; le gaz ambiant est de l'air pur. Les résultats de l'expérience et de la theorie indiquent tous les deux que le transport de chaleur diminue lorsque la vitesse du transport de masse à la paroi augmente. A des vitesses de soufflage modérées, il y a un bon accord entre les nombres de Nusselt déterminés expérimentalement et par la théorie. A des vitesses de transport de masse plus élevées, les données expérimentales se trouvent environ à 25% au-dessus des prévisions théoriques. Cet écart est attribué à un mouvement fluctuant dans la couche limite.

Zusammenfassung—Für freie Konvektion in einer Luft-Wasserdampf Grenzschicht am Staupunkt eines waagerechten Zylinders wird eine experimentelle Untersuchung zusammen mit einer Analyse beschrieben. Die zwei-Komponenten Grenzschicht wird durch Austreten von Wasserdampf aus der porösen Zylinderoberfläche erzeugt; das umgebende Gas ist reine Luft. Die Ergebnisse sowohl des Experiments als auch der Analyse zeigen, dass der Wärmeübergang abnimmt wenn der Stoffübergang an der Oberflache zunimmt. Für geringe Austrittsgeschwindigkeiten herrscht gute Übereinstimmung zwischen den experimentell und analytisch ermittelten Nusseltzahlen. Bei höhreren Stoffstromdichten liegen die Versuchsergebnisse etwa 25% über den analytischen Voraussagen. Diese Abweichung wird einer fluktuierenden Bewegung in der Grenzschicht zugeschrieben.

Аннотация—В статье описывается экспериментальное исследование вместе с расчетами свободной конвекции в пограничном слое воздухводяной пар в критической точке горизонтального цилиндра. Двухсоставной пограничный слой создается эффузией водяного пара из пористой поверхности цилиндра; окружающим газом является чистый воздух. Экспериментальные и расчетные результаты показывают, что теплообмен уменьшается с увеличением скорости теплообмена на поверхности. При не слишком больших скоростях сдувания найдено хорошее соответствие между числами Нуссельта, полученными экспериментально и теоретически. При более высоких скоростях теплообмена опытные данные превышают аналитические расчеты примерно на 25 процентов. Это отклонение объясняется флуктуациями в пограничном слое.